STIS UV Spectroscopy of Extreme Dust Candidate Sightlines

Scientific Category:	Stellar Populations and the Interstellar Medium
Scientific Keywords:	H II Regions, Interstellar Dust, Interstellar Medium, Polycyclic Aromatic Hydrocarbons
Instruments:	STIS
Exclusive Access Period:	6 months

Proposal Size: Small

Orbit Request	Prime	Parallel
Cycle 32	6	0

Abstract

Extinction and polarization by interstellar dust taints astrophysical signals, frustrating precision measurement of cosmological standard candles, electromagnetic components of multimessenger transients, and CMB signals. Understanding the origins of dust variations on small angular scales and along the line of sight in true three-dimensional detail, as informed by local physical influences, is now both possible and pressing. Cycle 29 STIS UV spectra of five stars in the immediate background of the well-studied O9.2IV star Zeta Oph revealed reddening curves with R_V=A_V/E(B-V)<2.4...among the most extreme known. The hard UV radiation field surrounding zeta Oph may be responsible for fragmenting dust and producing an excess of very small grains. Other physical influences, however, cannot be summarily dismissed. We propose STIS UV spectroscopy toward eight stars surrounding delta Sco, another nearby OB star where the radiative effects on dust can be probed in detail. With measurement of the near-UV reddening slope, the height and width of the 2175 A bump, and the far-UV rise, we will be able to forge a compelling association between extinction curve morphology and the proximity to a luminous star with a well-known emergent spectrum. Discovery of extreme reddening curves in another high-UV sightline would create a compelling association between radiative environment and dust size distribution. Characterizing the reddening in this local laboratory will enable understanding the conditions that produce anomalous dust in more distant AGN, SNe, GRB, and starburst environments.

Target Summary:

Target	RA	Dec	Magnitude
S1	16 01 54.5664	-23 01 14.95	10.92
S2	15 58 0.1128	-22 32 46.79	8.91
S3	15 58 36.9000	-22 57 15.55	10.76
S4	15 59 29.6424	-22 21 11.74	10.48
S5	16 00 41.3328	-22 35 31.70	11.22
S6	15 59 52.8648	-22 34 2.89	9.67
S7	16 01 12.9024	-22 13 16.14	11.42
S8	16 01 33.5520	-22 39 59.62	12.77

Observing Summary:

Target	Config Mode and Spectral Elements	Flags	Orbits
S1	STIS/NUV-MAMA Spectroscopic G230L (2376)		1
S2	STIS/NUV-MAMA Spectroscopic G230L (2376)		0
S3	STIS/NUV-MAMA Spectroscopic G230L (2376)		1
S4	STIS/NUV-MAMA Spectroscopic G230L (2376)		1
S5	STIS/NUV-MAMA Spectroscopic G230L (2376)		1
S6	STIS/NUV-MAMA Spectroscopic G230L (2376)		0
S7	STIS/NUV-MAMA Spectroscopic G230L (2376)		1
S8	STIS/NUV-MAMA Spectroscopic G230L (2376)		1

Total prime orbits: 6

Investigators:

Investigators and Team Expertise are included in this preview for your team to review. These will not appear in the version of the proposal given to the TAC, to allow for a dual anonymous review.

Role	Investigator	Institution	Country
CoI	Jordan Antoinette Bartlett	University of Wyoming	USA/WY
PI &	Dr. Henry A. Kobulnicky	University of Wyoming	USA/WY

Role	Investigator	Institution	Country
CoI	Brock Parker	University of Arizona	USA/AZ

Number of investigators: 3
& Contacts: 1

Team Expertise:

The PI is a 22nd year professor at an R1 university. He/She has supervised 12 PhD studentd and co-authored over 100 peer-reviewed publications. The PI and team of graduate students are active in spectroscopic and polarimetric investigations of the interstellar medium. The PI has led six HST programs since 1996.

CoI 1 is a 4th year PhD student at an R1 university. He/She is working on a dissertation involving dust propeties in various astrophysical environments. These proposed data may become part of the dissertation.

CoI 2 is a 1st year PhD student an an R1 university. He/She is leading a manuscript involving HST spectroscopic investigations of reddening toward highly irradiated ISM sightlines.

Scientific Justification

Dust grains permeate the interstellar medium, holding hostage the precious UV/optical/IR photometric precision that anchors astrophysical understanding. Dust both extincts and reddens the intrinsic spectral energy distributions of celestial targets in a manner that has been empirically characterized (e.g., Johnson 1965; Seaton 1979; Cardelli et al. 1989; Fitzpatrick et al. 2019) and theoretically approximated using a combination of silicate and carbonaceous (graphite) grains having a power-law distribution of radii between limits $a_{min} \lesssim 50$ Å — $a_{max} \approx 0.25$ μm (Mathis et al. 1977; Draine & Lee 1984; Draine & Li 2007). Established "standard" Milky Way reddening curves provide either the amount of extinction in magnitudes at wavelength λ relative to that at V band—A_λ/A_V (e.g., Cardelli et al. 1989, CCM89)—or the λ-V color excess normalized by the standard B-V excess—$k_\lambda \equiv$E(λ-V)/E(B-V) (e.g., Johnson 1965; Fitzpatrick et al. 2019, F19). **Figure 1** plots the latter representation as a function of inverse wavelength from the IR (left) through the ultraviolet (right). The typical curve (solid black line) traces a quasi-linear rise from the near-IR into the ultraviolet where a Lorentzian hump near 2175 Å results from a population of small graphite grains, producing elevated extinction (Stecher & Donn 1965; Li & Draine 2001; Weingartner & Draine 2001). The position of the 2175 Å feature is constant, suggesting a common carrier (likely polycyclic aromatic hydrocarbons, PAHs), but the strength and width and slope of the far-UV rise vary by sightline (Bless & Savage 1972; Fitzpatrick & Massa 1988; Gordon et al. 2009). An average reddening curve fails to capture the substantial variations known to exist along Galactic sightlines...a failure that impedes precision corrections required, for example, in cosmological SNe and γ-ray burst campaigns and cosmic microwave background calibration (Hoang 2017; Planck Collaboration et al. 2016, 2020; Brout & Scolnic 2021).

Reddening curves differ most dramatically in the IR and UV, as depicted by the labeled curves in Figure 1 and commonly parameterized by the ratio $R_V \equiv A_V$/E(B-V). While $R_V \approx 3.1$ represents an interstellar average, departures as extreme as $R_V = 2.1$ to $R_V = 6$ exist (Johnson 1965; Whittet et al. 1976; Larson et al. 2000) even along nearby sightlines (Wang et al. 2017), underscoring the importance of local physical conditions like UV irradiation and H_2 fraction on dust grain properties (Cardelli 1988; Rachford et al. 2009). Such dust is often termed 'anomalous' but the physical causes remain unclear. $R_V < 3.1$ curves exhibit a flatter IR extensions, larger 2175 Å bumps, and steeper far-UV rises. Physically, a preponderance of smaller grains and/or a deficit of larger grains produces less extinction in the IR and a more in the UV (Kim et al. 1994). Low-R_V sightlines are not as extensively documented as high-R_V sightlines, which usually pierce dark clouds. The best-studied is that through the diffuse cloud DBB80 toward the high-latitude B3V star HD210121 where $R_V \approx 2.1$ (Larson et al. 1996, 2000). Here, the wavelength of maximum polarization of optical background starlight shifts to smaller values $\lambda_{max} = 0.38$ μm compared to the interstellar average (≈ 0.55 μm), a signature of smaller grain sizes (Clayton & Cardelli 1988; Whittet et al. 1992). **Accurate dust corrections, especially in extreme environments (AGN, SNe, GRBs)**

require knowledge of the exact form of the reddening curve, but this precision has proven elusive, in part due to a dearth of good local laboratories.

Secure distances to reddened stars (i.e., *Gaia*, Gaia Collaboration et al. 2018) are empowering true three-dimensional reconstructions of the Galactic reddening in concert with a revolutionary capability to link variations in dust properties with local physical conditions. Historical studies of reddening in the Milky Way have relied upon OB stars on account of their copious UV fluxes and visibility to large distances, but the long path lengths to these targets inevitably sample a diverse admixture of dust populations. Cooler stars at lesser (but well-known) distances can also serve as valuable probes of dust on smaller angular scales and distances scales than rare early type stars. Cycle 29 HST STIS 1900–3200 Å UV spectra toward five F–G dwarfs in the immediate background of the nearby (d=182 pc) well-studied O9.2IV star ζ Oph revealed extreme reddening curves consistent with $R_{\rm V} \ll 3$. This luminous UV source produces an H II region with a radius of $\approx$16 pc (5° on the sky!), prominent in Hα images (Finkbeiner 2003; Haffner et al. 2003). Analysis of the UV data in concert with the optical and IR broadband measurements revealed that all five have exceptionally low $R_{\rm V}$ ranging from 1.4 to 2.5—among the lowest known! They also have weaker 2175 Å bumps. The result is robust when using any of three commonly adopted reddening curves (Fitzpatrick et al. 2019; Cardelli et al. 1989; Gordon et al. 2023). Indeed, these $R_{\rm V}$'s are lower than than all but one the most extreme OB stars used to *derive* standard reddening curves. ζ Oph itself, by contrast, has an "average" $R_{\rm V} \simeq 3.1$, based on historical literature (Bohlin et al. 1978) and authors' analysis of archival IUE spectra. **Figure 2** shows a schematic of the ζ Oph field illustrating the relative distances and results for the stars with HST STIS spectra. The nearest two background stars lie within 30 pc of ζ Oph, indicating that the anomalous dust component is located within this radius.

It is tempting to link the extraordinarily low $R_{\rm V}$ dust with the radiative influence of ζ Oph. This sightline exhibits prominent PAH emission striations at 8 μm (see *Spitzer* images in Piccone & Kobulnicky 2022), implicating ζ Oph's radiation field as the dominant influence on shaping dust grain properties in its vicinity. UV photons are expected to fragment dust grains, increasing the population of very small grains that produce elevated UV extinction and generating a population of PAHs responsible for broad mid-IR emission bands. Dust properties have been shown to vary as a function of distance from ionizing sources (Rapacioli et al. 2005; Berné et al. 2007; Peeters et al. 2017; Van De Putte et al. 2020). However, there could be other less obvious physical influences shaping the grain distribution along this particular sightline....shocks from unidentified supernovae, anomalous ambient radiation fields, cosmic rays above the Plane, etc. Therefore, additional measurements of reddening through similar UV-irradiated regions having a single dominant UV source are needed to test this hypothesis and identify the physical origins of anomalous dust.

The ISM surrounding δ Sco (B0.3IV) presents a similar laboratory to ζ Oph. As one of the nearest early type stars at d=152 pc, it generates a prominent H II region with a radius of

2° (5 pc). Proximity ensures that there are only 1–2 intervening ISM components (Welty & Hobbs 2001) so that confusion between multiple dust populations is less problematic than for distant targets that sample a wide range of physical conditions. Like ζ Oph, δ Sco lies 60 pc above the Galactic Plane at b=+23° and is reddened by a diffuse ISM component having E(B-V)$\simeq$0.18. Our analysis of archival IUE spectra with broadband optical and IR photometry yield R_V=3.06±0.21 (proposers, 2024), consistent with historical measurements (Wegner 2003) and consistent with "average" interstellar dust. At galactic longitude ℓ=350° it is sufficiently far from ζ Oph (ℓ=7°) that it constitutes a truly independent sightline. Its Galactic location allows for a larger number of warm background target stars to serve as probes of dust along closely bunched sightlines having transverse separations of <3 pc. Although δ Sco is a B0.3IV+B2V binary with a period of about 10.7 years (Bedding 1993; Tycner et al. 2011) its multiplicity is immaterial to the present study.

We propose STIS G230L spectroscopy of eight stars to measure the UV reddening curve through the δ Sco H II region along multiple sightlines. The UV portion of the spectrum is most sensitive to dust grain size distribution, as parameterized by R_V. From STIS G230L 1570–3180 Å spectra we propose to measure at least three of the four key features of the UV extinction curve: 1) the slope of the near UV rise, 2) the slope of the far-UV rise, 3) the height of the 2175 Å bump, and 4) potentially the width of the bump. The target stars lie within 30′ and bracket the δ Sco distance of 151 pc, with two stars in the foreground and six in the background to measure the reddening curve through its radiative sphere of influence. A discovery that the δ Sco sightlines exhibit non-standard low-R_V curves would provide strong evidence that UV photons—in this case by an unambiguous source having known spectral irradiance—plays the dominant role setting the grain size distribution, favoring enhanced populations of very small grains leading to elevated UV extinction. Deviations from the standard curve (e.g., LMC/SMC-like in **Figure 1**) would be equally interesting and would provide constraints for modeling the forces that shape grain distributions in irradiated environments. The LMC/SMC curves have been attributed either to increased UV flux, shocks, or the effects of lower metallicity (Misselt et al. 1999; Gordon et al. 2003). Some diffuse Galatic sightlines display weak bumps and steep far-UV rises where shocks are suspected (Clayton et al. 2000). If our targets show LMC/SMC-like curves with weak 2175 Å bumps, this would provide evidence that radiation rather than metallicity or shocks plays the dominant role.

Characterization of dust from reddening curves may be augmented by the addition of optical polarimetric data and optical spectroscopy of diffuse interstellar bands. R_V correlates with the wavelength of maximum interstellar polarization (Clayton & Cardelli 1988). The strengths and ratios of diffuse interstellar bands thought to be related to the grain size distribution and local radiation field (Jenniskens et al. 1994; Ramírez-Tannus et al. 2018). Our team is obtaining ground-based polarimetric and spectroscopic data in this field that

will help interpret the UV spectra within holistic picture of dust properties and radiation environment in a nearby accessible locale.

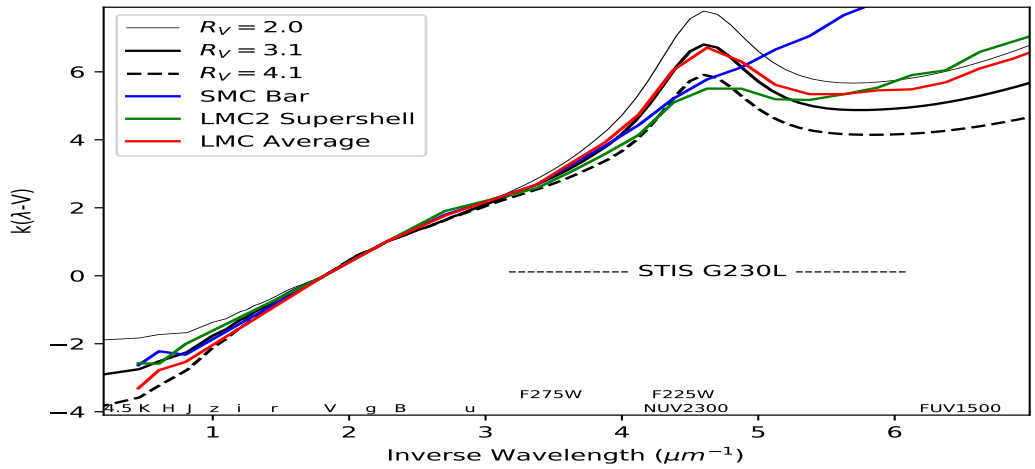

Figure 1: Canonical interstellar reddening curves (IR through UV) with variations parameterized by $R_V \equiv A_V/E(B\text{-}V)$. Colors depict SMC- and LMC-type curves.

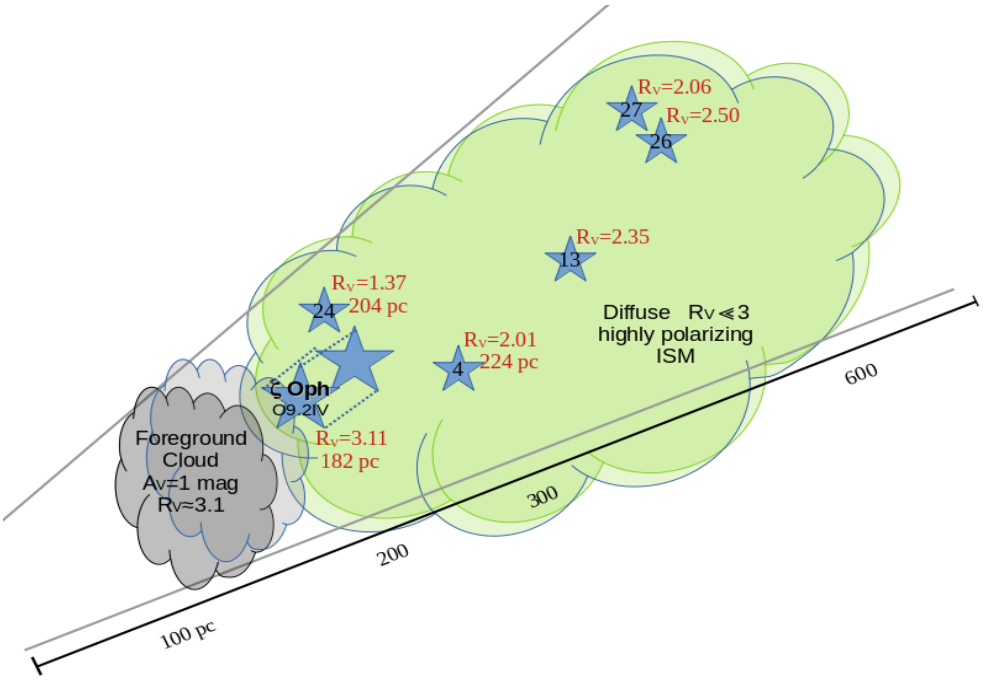

Figure 2: Stars in the immediate background of ζ Oph and within 30′separation have anomalously low R_V, based on Cycle 29 UV spectra—among the lowest R_V ever documented.

Description of the Observations

Observation Strategy and SNR Calculations

Our goal is to measure the reddening curve of the dust in and around the radiative influence of the B0.3IV star δ Sco A. Key features of the UV extinction curve to be measured are the slope of the near-UV rise, the height and width of the 2175 Å bump, and the far-UV slope.

We have selected eight stars within 30′ of δ Sco for STIS G230L spectroscopy covering 1570–3180 Å. Table 1 summarizes their positions, distances, Sloan g' magnitudes, effective temperatures, log(g), metallicity, E(B-V) color excesses, and expected exposure times. Five of the eight have Sloan IV APOGEE H-band spectra that yield very precise temperatures, gravities, metallicities, and color excesses that provide highly reliable expected fluxes at 2100 Å, the fiducial wavelength of interest just blueward of the 2175 Å bump. The other three stars have parameters from *Gaia* spectral template matching (*not* photometry) which correlate well with APOGEE stellar parameters for targets in common. All have high quality parallax distances and *Gaia* astrometry (RUWE¡1.4) consistent with single stars. All are selected to have no other *Gaia* sources within 3″ to avoid confusion issues with target acquisition or interpretation. An additional criterion is that they are bright enough (Sloan g' band) and hot enough to yield good signal-to-noise ratios near 2100 Å in reasonable exposure times. Two stars are slightly closer than δ Sco to serve as probes of the immediate foreground ISM; although archival IUE spectra of *delta* Sco itself are available, it is prudent to have independent measures of the foreground dust (apparently "average", based on IUE spectra and literature values) to mitigate against systematic calibration differences between IUE and HST/STIS (Bohlin & Bianchi 2018). Five of the stars lie in the 15–100 pc background of δ Sco to serve as probes of dust in and around its H II region in the same manner as the Cycle 29 STIS spectra toward ζ Oph. We selected one very distant star (985 pc) as a means of testing whether any unusual dust properties in the vicinity of δ Sco continue into the extra-planar (z >300 pc) Milky Way. **Figure 3** shows the locations of the targets in the δ Sco field.

Exposure times were selected to achieve a signal-to-noise ratio of 10:1 per resolution element at 2100 Å based on the known SED and reddening to each target using the HST/STIS exposure time calculator (ETC). We selected the G230L grating and adopted a 2″ slit to maximize throughput, as we care only about continuum slope and not about spectral resolution. We plan to bin the spectra into 30 Å bins (≈20 spectral pixels) for analysis purposes, resulting in SNRs of >25:1 at 2100 Å, sufficient to constrain at least three of the four key features of the reddening curve. Cycle 29 spectra of the ζ Oph field stars yielded only SNRs of 2:1 per resolution element at 2100 Å, on account of the cooler temperatures of available background targets in that field; those data were not sufficient to constrain the depth and width of the 2175 Å bump or the far-UV slope. By choosing brighter and hotter targets here with a larger SNR goal, we will be able to measure at least the near-UV and far-UV slope and probably

the width and depth of the 2175 Å bump, even if some averaging across targets is required. **Figure 4** (top panel) shows an example target spectrum (target S5) with the Y axis in photons per pixel as generated from the HST ETC for the proposed observation. Blue is the unreddened target after applying HST efficiencies. Magenta and green show the reddened spectrum for two different values of R_V. The grey band visible at shorter wavelengths shows the uncertainties per pixel. The lower panel of **Figure 4** shows the reddening curve recovered from the simulated observations; error bars shows pixel-by=pixel uncertainties propagated from the STIS ETC. Square symbols depict the data after 20-pixel averaging, illustrating the ability to distinguish two different reddening curves.

Given the 6+6+6 minute recommended allowances for guide star acquisition, target acquisition, and peakup for each target, the 8 targets can be observed in 6 orbits given that it appears possible to fit two short-exposure targets into a single orbit (S2 and S6 together and then S4 and S7).

Our analysis plan will also involve subtracting the reddening of δ Sco from the target stars to remove the foreground that may mask more extreme dust in the diffuse cloud at 150–200 pc distances. Similarly, the curve of the nearest stars will be compared to assess across-the-field variations, and then averaged to remove the nearest 150 pc dust from the more distant targets. Having eight targets is the minimum number to assess dust variations in two distance bins assuming uniform plane-of-sky properties or, alternately, two angular bins across-the-field of view to assess variations on the (projected) transverse scales of $<$3 pc at $\approx$200 pc distances.

Leveraging archival data: Owing to the proximity of the 2nd magnitude star δ Sco, there are no GALEX UV measurements of any stars in this field. However, there is a wealth of IUE archival spectra on δ Sco itself, which will be used in our analyses to subtract foreground reddening from the target stars.

Harnessing *HST*'s capabilities: The UV spectrum contains the most information about the nature of interstellar dust and is most sensitive to the morphology of the reddening curve for low-extinction translucent clouds. Obtaining UV spectra addressing the characteristics of extreme dust is a pressing task for *HST* during this waning age of UV spectroscopy.

Additional calibrations: None. The instrument setup is a well-used mode, so the standard wavelength calibration and flux calibrations will be adopted.

Complementary Data: Our team is acquiring ground-based optical spectrophotometry and multi-band polarimetry of additional stars in the field to measure the strength of diffuse interstellar bands that are known to be associated with PAHs and small grains (Ruiterkamp et al. 2002), and potentially with enhanced optical polarization or a shift in the wavelength of maximum polarization.

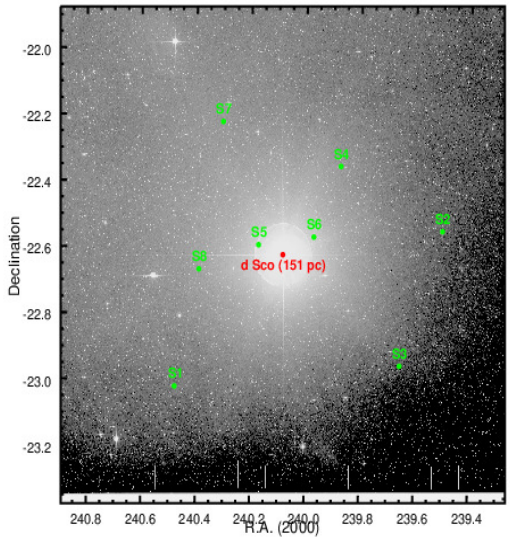

Figure 3: Locations of target stars within 30′ of δ Sco on a POSS R image.

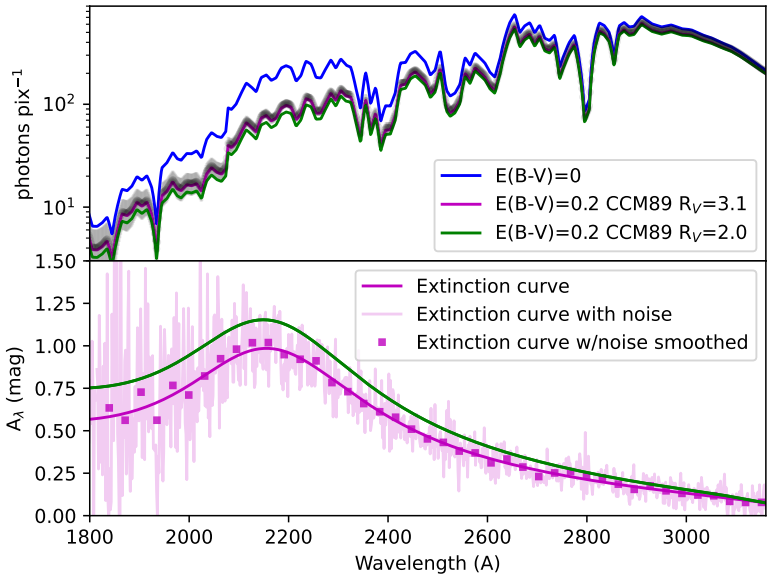

Figure 4: (Top) Simulated spectrum of target S5 from the HST/STIS ETC for two reddening curves normalized at 320 Å, with the grey band representing the pixel-by-pixel uncertainty from the ETC. Green shows $R_{\rm V}$=2.0 while magenta shows $R_{\rm V}$=3.1. (Bottom) Reddening curve recovered from the data by dividing a scaled theoretical model spectrum by the ETC simulated data. Error bars show the ETC expected S/N ratio. Squares show a 20-pixel block average.

Table 1: Targets surrounding δ Sco

ID	R.A.	Decl.	Gaia DR3#	d (pc)	$m_{g'}(mag)$	$T_{\rm eff}$ (K)	$E(B-V)$	Exp.(s)
S1	240.47736	-23.02082	6243123680760571648	125	10.92	5791	0.16	766
S2	239.50047	-22.54633	6237408934711867008	149	8.91	7193	0.20	7[a]
δ Sco				151			0.16	...
S3	239.65375	-22.95432	6237190612936085120	167	10.76	5830	0.18	734
S4	239.87351	-22.35326	6243410481494627456	207	10.48	6250	0.2	86
S5	240.17222	-22.59214	6243212500684771840	239	11.22	6500	0.2	113
S6	239.97027	-22.56747	6243210572238210432	340	9.67	7328	0.28	16
S7	240.30376	-22.22115	6243246585545445504	351	11.42	6634	0.21	155
S8	240.38980	-22.66656	6243197244960789888	985	12.77	6000	0.2	2400

[a]The brightest target S2 produces a warning that the maximum count rate exceeds 40% of the maximum allowable count rate for variable targets. Zwicky Transient Facility (ZTF) time-domain photometry confirms that this target is not variable by more than 0.02 mag.

Special Requirements

There are no timing, roll angle, or follow-on constraints.

Coordinated Observations

None.

Justify Duplications

None.

Analysis Plan

Not applicable for proposal type.

REFERENCES

Bedding, T. R. 1993, AJ, 106, 768, doi: 10.1086/116684

Berné, O., Joblin, C., Deville, Y., et al. 2007, A&A, 469, 575, doi: 10.1051/0004-6361:20066282

Bless, R. C., & Savage, B. D. 1972, ApJ, 171, 293, doi: 10.1086/151282

Bohlin, R. C., & Bianchi, L. 2018, AJ, 155, 162, doi: 10.3847/1538-3881/aaaec1

Bohlin, R. C., Savage, B. D., & Drake, J. F. 1978, ApJ, 224, 132, doi: 10.1086/156357

Brout, D., & Scolnic, D. 2021, ApJ, 909, 26, doi: 10.3847/1538-4357/abd69b

Cardelli, J. A. 1988, ApJ, 335, 177, doi: 10.1086/166918

Cardelli, J. A., Clayton, G. C., & Mathis, J. S. 1989, ApJ, 345, 245, doi: 10.1086/167900

Clayton, G. C., & Cardelli, J. A. 1988, AJ, 96, 695, doi: 10.1086/114838

Clayton, G. C., Gordon, K. D., & Wolff, M. J. 2000, ApJS, 129, 147, doi: 10.1086/313419

Draine, B. T., & Lee, H. M. 1984, ApJ, 285, 89, doi: 10.1086/162480

Draine, B. T., & Li, A. 2007, ApJ, 657, 810, doi: 10.1086/511055

Finkbeiner, D. P. 2003, ApJS, 146, 407, doi: 10.1086/374411

Fitzpatrick, E. L., & Massa, D. 1988, ApJ, 328, 734, doi: 10.1086/166332

Fitzpatrick, E. L., Massa, D., Gordon, K. D., Bohlin, R., & Clayton, G. C. 2019, ApJ, 886, 108, doi: 10.3847/1538-4357/ab4c3a

Gaia Collaboration, Brown, A. G. A., Vallenari, A., et al. 2018, A&A, 616, A1, doi: 10.1051/0004-6361/201833051

Gordon, K. D., Cartledge, S., & Clayton, G. C. 2009, ApJ, 705, 1320, doi: 10.1088/0004-637X/705/2/1320

Gordon, K. D., Clayton, G. C., Decleir, M., et al. 2023, ApJ, 950, 86, doi: 10.3847/1538-4357/accb59

Gordon, K. D., Clayton, G. C., Misselt, K. A., Landolt, A. U., & Wolff, M. J. 2003, ApJ, 594, 279, doi: 10.1086/376774

Haffner, L. M., Reynolds, R. J., Tufte, S. L., et al. 2003, ApJS, 149, 405, doi: 10.1086/378850

Hoang, T. 2017, ApJ, 836, 13, doi: 10.3847/1538-4357/836/1/13

Jenniskens, P., Ehrenfreund, P., & Foing, B. 1994, A&A, 281, 517

Johnson, H. L. 1965, ApJ, 141, 923, doi: 10.1086/148186

Kim, S.-H., Martin, P. G., & Hendry, P. D. 1994, ApJ, 422, 164, doi: 10.1086/173714

Larson, K. A., Whittet, D. C. B., & Hough, J. H. 1996, ApJ, 472, 755, doi: 10.1086/178104

Larson, K. A., Wolff, M. J., Roberge, W. G., Whittet, D. C. B., & He, L. 2000, ApJ, 532, 1021, doi: 10.1086/308619

Li, A., & Draine, B. T. 2001, ApJ, 554, 778, doi: 10.1086/323147

Mathis, J. S., Rumpl, W., & Nordsieck, K. H. 1977, ApJ, 217, 425, doi: 10.1086/155591

Misselt, K. A., Clayton, G. C., & Gordon, K. D. 1999, ApJ, 515, 128, doi: 10.1086/307010

Peeters, E., Bauschlicher, Charles W., J., Allamandola, L. J., et al. 2017, ApJ, 836, 198, doi: 10.3847/1538-4357/836/2/198

Piccone, A. N., & Kobulnicky, H. A. 2022, ApJ, 924, 138, doi: 10.3847/1538-4357/ac36d8

Planck Collaboration, Ade, P. A. R., Aghanim, N., et al. 2016, A&A, 586, A141, doi: 10.1051/0004-6361/201526506

Planck Collaboration, Akrami, Y., Ashdown, M., et al. 2020, A&A, 641, A11, doi: 10.1051/0004-6361/201832618

Rachford, B. L., Snow, T. P., Destree, J. D., et al. 2009, ApJS, 180, 125, doi: 10.1088/0067-0049/180/1/125

Ramírez-Tannus, M. C., Cox, N. L. J., Kaper, L., & de Koter, A. 2018, A&A, 620, A52, doi: 10.1051/0004-6361/201833340

Rapacioli, M., Joblin, C., & Boissel, P. 2005, A&A, 429, 193, doi: 10.1051/0004-6361:20041247

Ruiterkamp, R., Halasinski, T., Salama, F., et al. 2002, A&A, 390, 1153, doi: 10.1051/0004-6361:20020478

Seaton, M. J. 1979, MNRAS, 187, 73, doi: 10.1093/mnras/187.1.73P

Stecher, T. P., & Donn, B. 1965, ApJ, 142, 1681, doi: 10.1086/148461

Tycner, C., Ames, A., Zavala, R. T., et al. 2011, ApJ, 729, L5, doi: 10.1088/2041-8205/729/1/L5

Van De Putte, D., Gordon, K. D., Roman-Duval, J., et al. 2020, ApJ, 888, 22, doi: 10.3847/1538-4357/ab557f

Wang, S., Jiang, B. W., Zhao, H., Chen, X., & de Grijs, R. 2017, ApJ, 848, 106, doi: 10.3847/1538-4357/aa8db7

Wegner, W. 2003, Astronomische Nachrichten, 324, 219, doi: 10.1002/asna.200310081

Weingartner, J. C., & Draine, B. T. 2001, ApJ, 548, 296, doi: 10.1086/318651

Welty, D. E., & Hobbs, L. M. 2001, ApJS, 133, 345, doi: 10.1086/320354

Whittet, D. C. B., Martin, P. G., Hough, J. H., et al. 1992, ApJ, 386, 562, doi: 10.1086/171039

Whittet, D. C. B., van Breda, I. G., & Glass, I. S. 1976, MNRAS, 177, 625, doi: 10.1093/mnras/177.3.625